

## THE ABUNDANCE OF CO IN DIFFUSE INTERSTELLAR CLOUDS— AN ULTRAVIOLET SURVEY

S. R. FEDERMAN AND A. E. GLASSGOLD  
 New York University Physics Department

AND

EDWARD B. JENKINS AND EDWARD J. SHAYA  
 Princeton University Observatory

Received 1980 April 24; accepted 1980 June 4

### ABSTRACT

An ultraviolet survey of interstellar CO has been made with *Copernicus* in the  $C-X$  1088 Å and  $E-X$  1076 Å lines toward 48 bright stars. CO was detected in 17 directions, and upper limits were estimated for 21 others. Nine of the detections involve unsaturated features from which column densities are deduced. An overall picture of CO column densities toward bright stars is obtained by combining these results with those of other *Copernicus* investigations made with weaker transitions. The CO column densities are in the range  $10^{12}$ – $10^{15}$  cm<sup>-2</sup>, and they correlate well with those of C I and H<sub>2</sub>, varying roughly as the first and second power, respectively. Theoretical considerations and calculations are also given which suggest that the overall trends of the UV observations are in accord with current concepts of gas phase chemistry. Evidence for the predicted dependences of the CO abundance on H<sub>2</sub> abundance and on dust column density are adduced. The tendency of the C I/CO ratio to be about 10 for this sample is shown to follow from the ratio of particular atomic and molecular cross sections as well as from the values of the physical parameters of interstellar clouds. The connection between UV observations of CO in diffuse clouds and radio observations of <sup>13</sup>CO in dark clouds is also discussed. When fractionation is taken into account, all of the data in the range  $10^{19}$  cm<sup>-2</sup>  $\lesssim N(\text{H}_2) \lesssim 10^{22}$  cm<sup>-2</sup> appear to form a continuum.

*Subject headings:* interstellar: abundances — interstellar: molecules — ultraviolet: spectra

### I. INTRODUCTION

Carbon monoxide is the most abundant and widespread heavy molecule observed in the interstellar medium. It was discovered by Wilson, Jefferts, and Penzias (1970) in emission at 115 GHz from gas clouds associated with H II regions. The ultraviolet absorption lines were first detected toward ζ Oph by Smith and Stecher (1971), and then toward several other early type stars by Jenkins, Drake, *et al.* (1973) with the *Copernicus* satellite. The astrophysical importance of CO stems from its physical and chemical properties. The scale of its rotational spectrum ( $B = 2.766$  K) is such that the energy level separations correspond to the temperatures of interstellar clouds; hence CO can be an important coolant. The theoretical calculation of the abundance of CO represents an important challenge to interstellar chemistry, if only because such a large amount of carbon is incorporated in this one molecule. The radio emission from CO is especially useful as a tracer for the structure and kinematics of complexes of molecular clouds (Scoville, Solomon, and Penzias 1975; Kutner *et al.* 1977; Elmegreen, Lada, and Dickinson 1979; Loren 1979) and for ascertaining the distribution of such clouds in the Galaxy (Scoville and Solomon 1975; Gordon and Burton 1976; Solomon, Scoville, and Sanders 1979).

Despite many observational studies of CO, especially at radio frequencies, its abundance relative to hydrogen is not well established. Part of the problem is that the lines are frequently saturated, both at ultraviolet and at radio frequencies. Thick clouds ( $A_v > 1$ ) present a special problem because the main gaseous component, molecular hydrogen, cannot be measured directly.

In this article we present the results of an extensive ultraviolet survey of CO made with the *Copernicus* satellite in the strong  $v' = 0 \rightarrow v = 0$  transitions at  $\lambda = 1088$  Å ( $C^1\Sigma^+ - X^1\Sigma^+$ ,  $f = 0.089$ ) and  $\lambda = 1076$  Å ( $E^1\Pi - X^1\Sigma^+$ ,  $f = 0.12$ ). Detections of CO were made for about one-third of the 48 spectral scans of bright stars. Some of the detected lines were saturated so that only lower limits could be obtained to the column densities of CO. In many of these cases we were able to obtain column densities from observations of weaker lines by other workers, both published (Morton 1975; Morton and Hu 1975; Snow 1975, 1977) and to be published (Snow and Jenkins 1980). Consequently we are able to present CO column densities for clouds with a wide range of (atomic and molecular) hydrogen column densities. We will discuss these determinations for diffuse clouds ( $A_v \lesssim 1$ ) in relation to radio observations of CO for thicker clouds ( $A_v \gtrsim 1$ ) and in the context of theoretical calculations.

The plan of the rest of this report is as follows. In § II we discuss the data and how they have been analyzed. In § III we present the results graphically in several ways, and discuss their significance with the help of simple theoretical concepts.

The relation between UV and radio observations is taken up in § IV, and some conclusions and general remarks make up the contents of the last section V.

## II. DATA AND ANALYSIS

The spectra for this survey were obtained during the first half-year of operation of the *Copernicus* satellite with the high-resolution U1 phototube. Scans were made in order to search for the 0-0 bands of the *C-X* and *E-X* transitions of CO in absorption at 1087.867 Å and 1076.033 Å, respectively. Interstellar CO was detected in 17 of the 48 lines of sight which were investigated. The marginal detection of a feature toward  $\iota$  Ori may be due to some other species shifted into the spectrum by high velocity gas. Upper limits to the column density of CO in 21 directions also have been obtained. The spectra for the 10 remaining directions yielded no useful information on interstellar CO. In most of the latter cases, the star's projected rotation velocity was small ( $v \sin i < 70 \text{ km s}^{-1}$ )—leading to confusion with stellar features. A typical high quality *C-X* 1088 Å absorption spectrum may be seen in Figure 1 of Jenkins, Drake, *et al.* (1973). The *E-X* 1076 Å spectra are generally inferior; they were used mainly to confirm results deduced from the 1088 Å spectra. In no case did we obtain a statistically significant detection at 1076 Å without a detection at 1088 Å. The *C-X* spectra have two characteristic properties which are useful for the detection of interstellar CO. As noted by Jenkins, Drake, *et al.* (1973), there is a strong unidentified line at 1088.07 Å, which is associated with the CO feature.<sup>1</sup> In every spectrum where we report a detection, there is evidence—frequently striking—of this mystery feature. There are no 1088 Å spectra with only a single feature, which could have caused us to confuse CO with some other species. The second property of the 1088 Å spectra is that the rotational splitting is partially resolved in many cases. In the best cases, the main *R*(0) line, the partially resolved and blended *P*(1) line, and the mystery feature present a triple pattern with a regular separation of 100 mÅ. In other cases, the rotational structure is spread out, and the CO signature is a rotationally broadened line located 200 mÅ shortward of a fairly symmetric, unidentified line. Such regular patterns provide a reliable basis for the detection of interstellar CO. The rotational splittings are of the same order (or less) as the resolution of the spectrometer, so that the relatively low quality of the scans does not justify a detailed analysis in terms of the rotational level populations. Also, conclusions on the distribution of rotational populations are very sensitive to whether or not the lines are saturated. Instead, total equivalent widths, integrated over the entire line shape, have been obtained.

We adopted the following procedure for deriving the equivalent widths and their errors. Changed particle backgrounds were estimated using the standard procedures described by York and Miller (1974). Many of our scans had large stray light contributions adding to the background, since the data were recorded before the spectrometer scanning procedures were reprogrammed to eliminate the contribution of signal reaching the U1 detector through its vent hole. Hence, we had to correct for the elevation of the zero baseline with the procedures outlined by York (1972). Corrections for scattered light from the grating were also carried out, using the formula of Bohlin (1975). Aside from possible systematic uncertainties in the aforementioned corrections, two principal sources of error for the equivalent widths are (a) the random fluctuations in signal caused by photon counting and (b) the uncertainty in the placement of the continuum level. Jenkins, Drake, *et al.* (1973) give a formula for the magnitude of the error caused by counting statistics, assuming that the continuum is accurately known. We have adopted this formula with  $M = 6$  (the number of U1 steps included in the equivalent width integration) to express the magnitude of this error  $\epsilon_w$ . Unlike most interstellar lines, the CO features are not especially narrow or easy to define. Hence the determination of a good continuum was often difficult, especially if the stellar flux changed markedly with wavelength. For each spectrum, lower and upper extremes for the continuum curves were estimated independently by two of us (S. R. F. and A. E. G.), and the resulting effect on the equivalent width measurement was used to determine the expected error from faulty continuum placement  $\epsilon_c$ . For many of the detected CO features,  $\epsilon_c$  was greater than  $\epsilon_w$ . A combined  $1 \sigma$  error  $\epsilon$  was evaluated from the expression  $\epsilon = (\epsilon_w^2 + \epsilon_c^2)^{1/2}$ .

Equivalent widths were measured over an interval of about 150 mÅ for all spectral scans, irrespective of whether or not an absorption feature could be seen. If the formal measurement  $W$  did not exceed  $2\epsilon$ , we quoted an upper limit for the width equal to  $W + 2\epsilon$ . To be conservative, we specified positive, definite values for widths only when  $W > 2\epsilon$  and the visual appearance of the tracing indeed suggested the presence of a CO feature of approximately the right shape.

A conservative position also was adopted in converting equivalent widths to column densities. As discussed above, the observations yield a single equivalent width, usually for the 1088 Å transition. We do not have a curve of growth, and thus are unable to determine CO column densities except for optically thin lines. For the *C-X* 1088 Å transition, we derive equivalent widths from

$$N(\text{CO}) = 1.07[W_{1088}/\text{mÅ}][f/0.089]^{-1} \times 10^{12} \text{ cm}^{-2} \quad (1)$$

only if  $W_{1088} \lesssim 10 \text{ mÅ}$ , which corresponds to  $N(\text{CO}) \lesssim 10^{13} \text{ cm}^{-2}$ . When  $W_{1088} > 10 \text{ mÅ}$ , we use (1) to obtain a lower limit (based on  $W - 2\epsilon$ ). The corresponding formula for the *E-X* 1076 Å transition is

$$N(\text{CO}) = 0.813[W_{1076}/\text{mÅ}][f/0.12]^{-1} \times 10^{12} \text{ cm}^{-2} . \quad (2)$$

<sup>1</sup> Some authors believe this feature arises from Cl I, but see Morton (1979) for a dissenting view.

TABLE 1  
CO EQUIVALENT WIDTHS AND COLUMN DENSITIES

HD (1)	Name (2)	$W_{1088}$ (mÅ) (3)	$W_{1076}$ (mÅ) (4)	$N(\text{CO})$ ( $\text{cm}^{-2}$ ) (this work) (5)	$N(\text{CO})$ ( $\text{cm}^{-2}$ ) (other work) (6)	$\text{H} + 2\text{H}_2^a$ ( $\text{cm}^{-2}$ ) (7)	$\text{H}_2^a$ ( $\text{cm}^{-2}$ ) (8)	$\text{C I}^b$ ( $\text{cm}^{-2}$ ) (9)	Notes (10)
14228	..... $\phi$ Eri	$1.6 \pm 1.7$	$0.3 \pm 2.3$	$< 5.4(12)$	...	...	$< 1(17)$	...	
21278	..... ...	$21 \pm 3$	$7^{+5}_{-4}$	$> 1.6(13)$	...	$> 6.0(19)$	$3.0(19)$	$> 1.07(14)$	
23180	..... $\sigma$ Per	$61^{+7}_{-6}$	$74 \pm 5$	$> 5.3(13)$	$6.5^{+2.4}_{-1.7}(14)$	$1.61(21)$	$4.0(20)$	$4.7 \pm 0.8(15)$	c
23408	..... 20 Tau	$32 \pm 8$	...	$> 1.7(13)$	...	$> 1.1(20)$	$5.6(19)$	...	
23630	..... $\eta$ Tau	$2.8 \pm 2.4$	$0.8 \pm 2.4$	$< 8.1(12)$	...	$> 6.9(19)$	$3.5(19)$	...	
24398	..... $\zeta$ Per	$48 \pm 7$	$40 \pm 6$	$> 3.6(13)$	$7.2^{+3.3}_{-2.3}(14)$	$1.58(21)$	$4.7(20)$	$3.3 \pm 0.2(15)$	d
24760	..... $\varepsilon$ Per	$8 \pm 2$	$1.3^{+0.8}_{-0.6}$	$9 \pm 2(12)$	...	$3.2(20)$	$3.3(19)$	$4.7 \pm 1.4(13)$	
24912	..... $\xi$ Per	$31 \pm 2.5$	$26 \pm 2$	$> 2.8(13)$	...	$1.98(21)$	$3.4(20)$	$2.6 \pm 1.0(15)$	
28497	..... ...	$0.4 \pm 1.2$	$1.8 \pm 2.0$	$< 4.7(12)$	...	$1.60(20)$	$6.6(14)$	...	
36486	..... $\delta$ Ori	$0.4 \pm 0.2$	$0.6 \pm 0.4$	$< 1.1(12)$	...	$1.70(20)$	$4.8(14)$	$< 1.7(13)$	e
37043	..... $\iota$ Ori	$2.5 \pm 0.6$	$0.9 \pm 0.6$	$2.7^{+1.2}_{-0.9}(12)$	...	$1.40(20)$	$4.9(14)$	$6.9 \pm 1.8(12)$	e
37128	..... $\varepsilon$ Ori	$0.9 \pm 0.5$	$0.5 \pm 0.5$	$< 2.0(12)$	...	$2.8(20)$	$3.7(16)$	$2.8 \pm 0.4(13)$	e
37202	..... $\zeta$ Tau	$0.8 \pm 0.6$	$0.1 \pm 0.2$	$< 2.1(12)$	...	$1.10(20)$	$< 4.7(17)$	...	
37742	..... $\zeta$ Ori	$1.0^{+1.0}_{-0.5}$	$-1.5 \pm 4.0$	$< 5.3(12)$	...	$2.6(20)$	$5.4(15)$	$5.9 \pm 1.2(13)$	e
40111	..... 139 Tau	$4.0 \pm 2.8$	$-0.2 \pm 2.2$	$< 1.0(13)$	...	$9.1(20)$	$5.4(19)$	...	
47839	..... 15 Mon	$0.5 \pm 1.0$	$4.0 \pm 2.0$	$< 6.5(12)$	...	$2.5(20)$	$3.5(15)$	$< 3.6(13)$	e
53138	..... $\sigma^2$ CMa	$4.0 \pm 2.4$	...	$< 9.4(12)$	...	$1.5(20)$	...	$1.6 \pm 0.7(13)$	e
57060	..... 29 CMa	$0.7 \pm 1.1$	$3.0 \pm 1.4$	$< 4.7(12)$	...	$5.0(20)$	$6.0(15)$	$< 2.6(13)$	
57061	..... $\tau$ CMa	$1.4 \pm 1.2$	$0.2 \pm 0.8$	$< 4.1(12)$	...	$5.0(20)$	$3.0(15)$	$> 3.2(13)$	e
66811	..... $\zeta$ Pup	$0.4 \pm 0.4$	...	$< 1.3(12)$	...	$9.7(19)$	$2.8(14)$	...	
68273	..... $\gamma^2$ Vel	$1.1 \pm 0.8$	$-0.5 \pm 0.4$	$< 2.9(12)$	...	$6.0(19)$	$1.7(14)$	$< 2.0(13)$	
87901	..... $\alpha$ Leo	$0.3 \pm 0.75$	$-0.3 \pm 1.0$	$< 1.9(12)$	...	...	$< 9.5(14)$	...	
91316	..... $\rho$ Leo	$2.0 \pm 1.8$	$1.5 \pm 1.6$	$< 6.0(12)$	...	$1.8(20)$	$4.1(15)$	$2.2 \pm 0.5(13)$	
93030	..... $\theta$ Car	$0.2 \pm 0.3$	...	$< 9(11)$	...	$1.9(20)$	$< 4.5(17)$	$> 1.3(13)$	
135742	..... $\beta$ Lib	$0.4 \pm 2.2$	...	$< 5.1(12)$	...	...	$< 2.2(14)$	...	
143018	..... $\pi$ Sco	$0.8 \pm 0.2$	...	$9 \pm 3(11)$	...	$5.6(20)$	$2.1(19)$	$8.1 \pm 2.2(12)$	
143275	..... $\delta$ Sco	$6.0 \pm 0.8$	...	$6.4 \pm 0.9(12)$	$9 \pm 2(12)$	$1.45(21)$	$2.6(19)$	$2.2 \pm 0.2(14)$	f
144470	..... $\omega'$ Sco	$12 \pm 1.6$	...	$1.3 \pm 0.2(13)$	$4.0 \pm 0.8(13)$	$1.73(21)$	$1.13(20)$	$9.6 \pm 0.9(13)$	f
145502	..... $\nu$ Sco	$5.0^{+3.3}_{-2.1}$	...	$5.4^{+3.3}_{-2.3}(12)$	$4.0 \pm 0.8(13)$	$1.56(21)$	$7.8(19)$	$5.7 \pm 1.5(14)$	f
147933	..... $\rho$ Oph A	$22 \pm 7$	...	$> 9(12)$	$6.0 \pm 2.4(14)$	$7.24(21)$	$3.7(20)$	$3.3 \pm 1.4(15)$	f
149038	..... $\mu$ Nor	$39^{+8.4}_{-5.1}$	...	$> 3.1(13)$	...	$1.56(21)$	$2.8(20)$	$> 3.0(14)$	
149757	..... $\zeta$ Oph	...	$34^{+5.2}_{-4.2}$	$> 2.1(13)$	$2.2 \pm 0.4(15)$	$1.41(21)$	$4.4(20)$	$3.2 \pm 0.2(15)$	g
158408	..... $\nu$ Sco	$-0.8 \pm 0.3$	...	...	...	$< 1.8(19)$	$< 1.3(14)$	...	
164353	..... 67 Oph	$10^{+7}_{-6}$	$8 \pm 4$	$8 \pm 5(12)$	...	$1.37(21)$	$1.83(20)$	...	
175191	..... $\sigma$ Sqr	$0.7 \pm 0.5$	$0.2 \pm 0.3$	$< 1.8(12)$	...	$< 3(19)$	$< 1.0(14)$	...	
200120	..... 59 Cyg	$5.0 \pm 1.5$	$0.9 \pm 1.4$	$5.4 \pm 1.6$	...	$2.2(20)$	$2.0(19)$	...	
209952	..... $\alpha$ Gru	$0.0 \pm 0.8$	$0.1 \pm 0.8$	$< 1.7(12)$	...	...	$< 4.8(13)$	...	
217675	..... $\sigma$ And	$12 \pm 2$	$10 \pm 3$	$1.1 \pm 0.2(13)$	...	$> 9.4(19)$	$4.7(19)$	$5.1 \pm 1.2(13)$	h

<sup>a</sup> The column densities of H and H<sub>2</sub> were determined by Copernicus ultraviolet investigations of Savage *et al.* 1977 and Bohlin *et al.* 1978.

<sup>b</sup> The C I column densities were determined with Copernicus by Jenkins and Shaya 1979.

<sup>c</sup> Lower limit derived from both 1088 and 1076 spectra with weights proportioned to  $\varepsilon^{-1}$ . Other measurement is B-X (Snow 1975).

<sup>d</sup> Other measurement is B-X (Snow 1977).

<sup>e</sup> C I column density subjected to significant correction from accompanying H II region (Jenkins and Shaya 1979).

<sup>f</sup> Other measurement is B-X (Snow and Jenkins 1980).

<sup>g</sup> Other measurement is based on a reanalysis of Morton's A-X equivalent widths (1975) and revised oscillator strengths.

<sup>h</sup> Column density is average of 1076 and 1088 results, weighted according to  $\varepsilon^{-1}$ .

Equations (1) and (2) are based on oscillator strengths determined by Smith (1978) from lifetime measurements. His results are in agreement with earlier results by Hesser (1968) and Pilling, Boss, and Brown (1971), but about a factor of 2 smaller than those derived from electron scattering by Lassetre and Skeberle (1971). This systematic deviation of the electron scattering results is well known, and arises from the Born approximation treatment of the excitation process.

The results of the data analysis are presented in Table 1 along with related results obtained from previous Copernicus investigations. The errors are the *one* standard deviation parameter. We shall discuss these results in detail in the next section.

### III. RESULTS AND INTERPRETATION

We base our discussion of the data in Table 1 on graphical intercomparisons of CO with measured column densities of other closely related species and on comparisons with theoretical calculations. Plots of CO versus H<sub>2</sub> are given in Figures 1 and 2, whereas Figure 3 gives CO versus total hydrogen column density  $N \equiv N(\text{H}) + 2N(\text{H}_2)$ , and Figure 4 gives CO

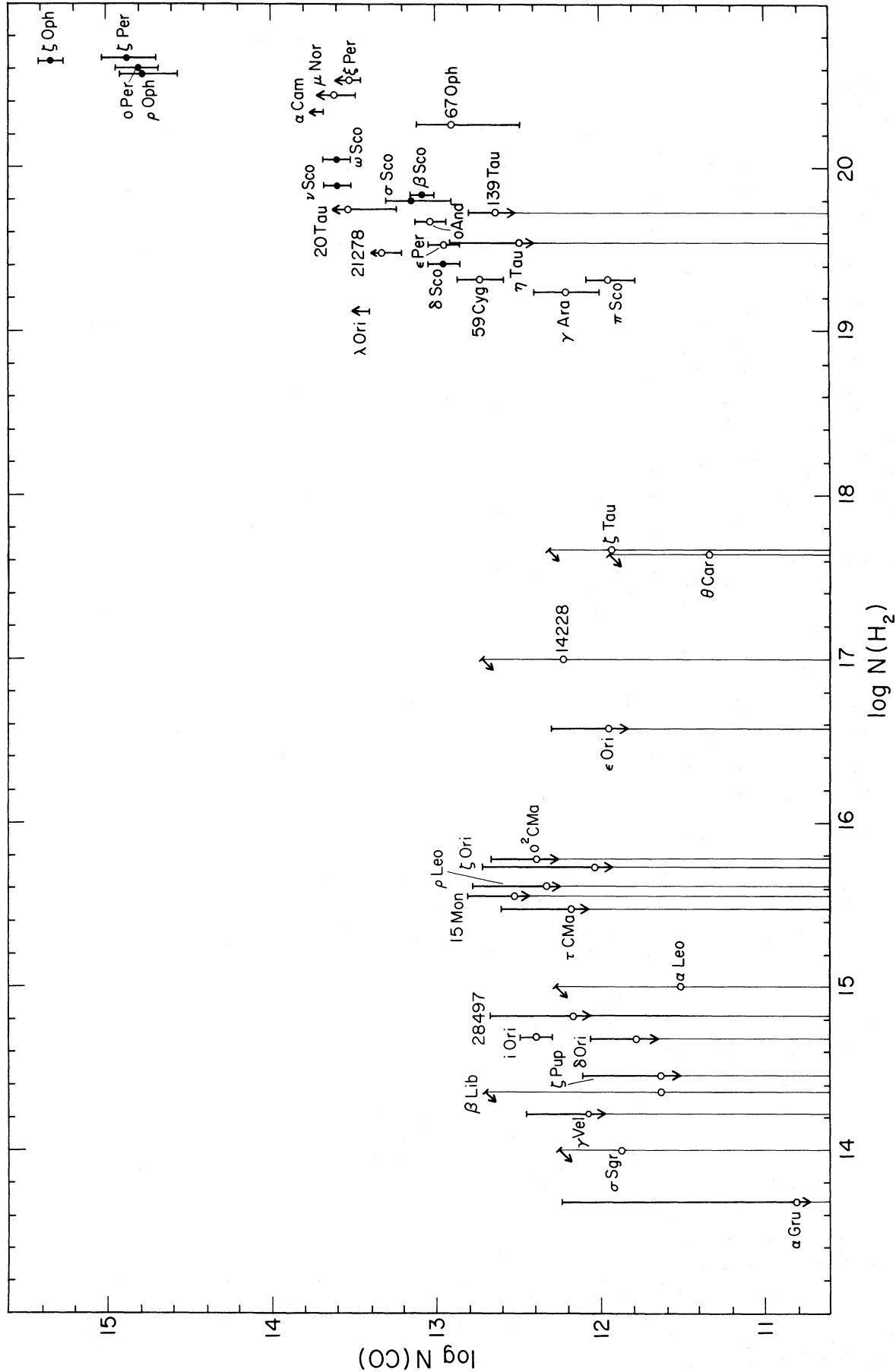


FIG. 1.—CO vs. H<sub>2</sub> column densities. The open circles refer to the strong C-X and E-X transitions used in this survey, supplemented by a few earlier measurements as described in the text. The filled circles are measurements obtained by other workers from the weaker B-X and, for  $\zeta$  Oph only, A-X transitions. The error bars represent  $\pm$  one standard deviation. Upper and lower limits are indicated by arrows, and the formal value of the column density is given by the open circle. Slant arrows have been used in those cases where only upper limits to the column density of molecular hydrogen are available.

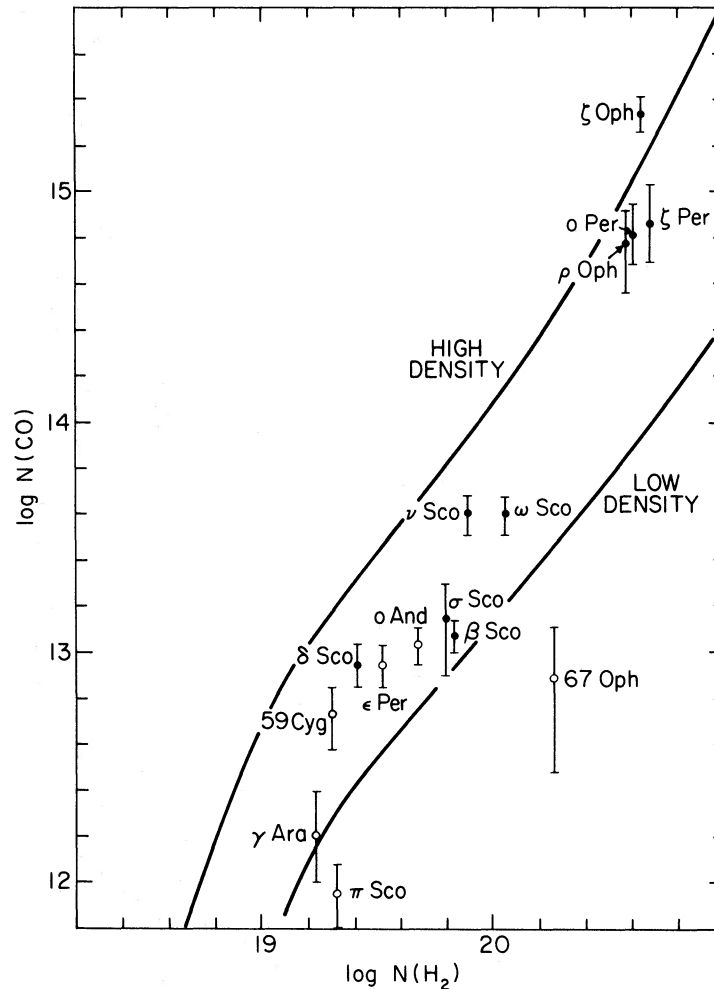


FIG. 2.—CO vs.  $H_2$  column density measurements for  $10^{19} \text{ cm}^{-2} \lesssim N(H_2) \lesssim 10^{21} \text{ cm}^{-2}$ . Solid lines, theoretical calculations discussed in § IIIb of the text for the parameter sets in Table 3.

versus C I. Two typical theoretical calculations will be used, and will be referred to as the “low density” and the “high density” models. The two calculations roughly bracket the data. They are based on an updated version of the steady-state, isobaric model of Glassgold and Langer (1974, 1976) which includes the latest information on the relevant ion-molecule reactions and other physical processes (Federman and Glassgold 1980). The parameters for the calculations are given in Table 2. Because the temperature and density vary, both mean values and ranges for these parameters are given for the regions where most of the CO is located.

The open circles in Figures 1–3 are based upon the strong C–X and E–X transitions observed in this work, except for  $\alpha$  Cam and  $\lambda$  Ori (Jenkins, Drake, *et al.* 1973) and  $\gamma$  Ara (Morton and Hu 1975). The filled circles were determined by other *Copernicus* investigators from the weaker B–X and, for  $\zeta$  Oph only, A–X transitions; references are given in the notes to Table 1. (For these directions we made no attempt to convert our equivalent widths for saturated C–X and E–X transitions into column densities.) The results of Snow and Jenkins (1980) for  $\beta$  Sco and  $\sigma$  Sco also have been plotted. Upper and lower limits for our own data are indicated by arrows in Figures 1 and 3, whereas Figure 2 only includes actual values of column densities and no limits.

#### a) CO and $H_2$

A broad overview of all of the data is given in Figure 1, where column densities of CO are plotted against those for  $H_2$  on a log-log plot. One general conclusion is immediately clear: CO is readily detected where substantial amounts of  $H_2$  are observed. For *Copernicus* observations, this means roughly  $N(H_2) > 10^{19} \text{ cm}^{-2}$ . [The only directions with  $N(H_2) > 10^{19} \text{ cm}^{-2}$  where CO was *not* detected are toward  $\eta$  Tau and 139 Tau, but the upper limits in these cases are not much below the other detections in Fig. 1.] A second general conclusion from Figure 1 is that the measured CO column

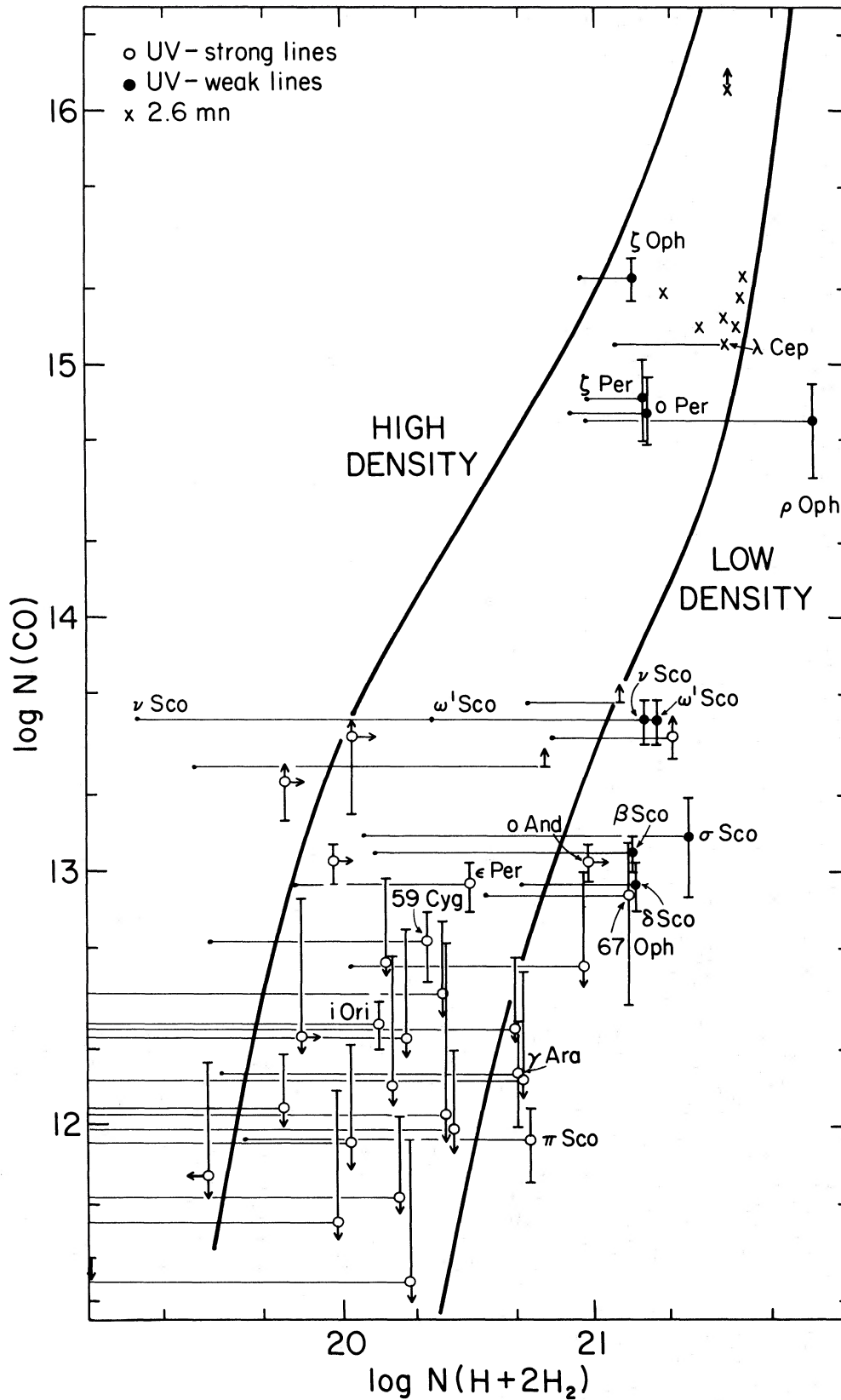


FIG. 3.—CO vs. total hydrogen column density  $N \equiv N(\text{H} + 2\text{H}_2) \equiv N(\text{H}) + 2N(\text{H}_2)$ . The representation is essentially the same as in Fig. 1. The dots at the end of the light horizontal line are where  $N = 2N(\text{H}_2)$ . Crosses, the radio observations of Knapp and Jura (1976). An upper limit for  $\mu$  Nor could not be plotted because it would coincide with the detection for  $\nu$  Sco. In order to reduce crowding, only the names of stars for which detections have been made are included. Solid lines, theoretical calculations described in § IIIb of the text.

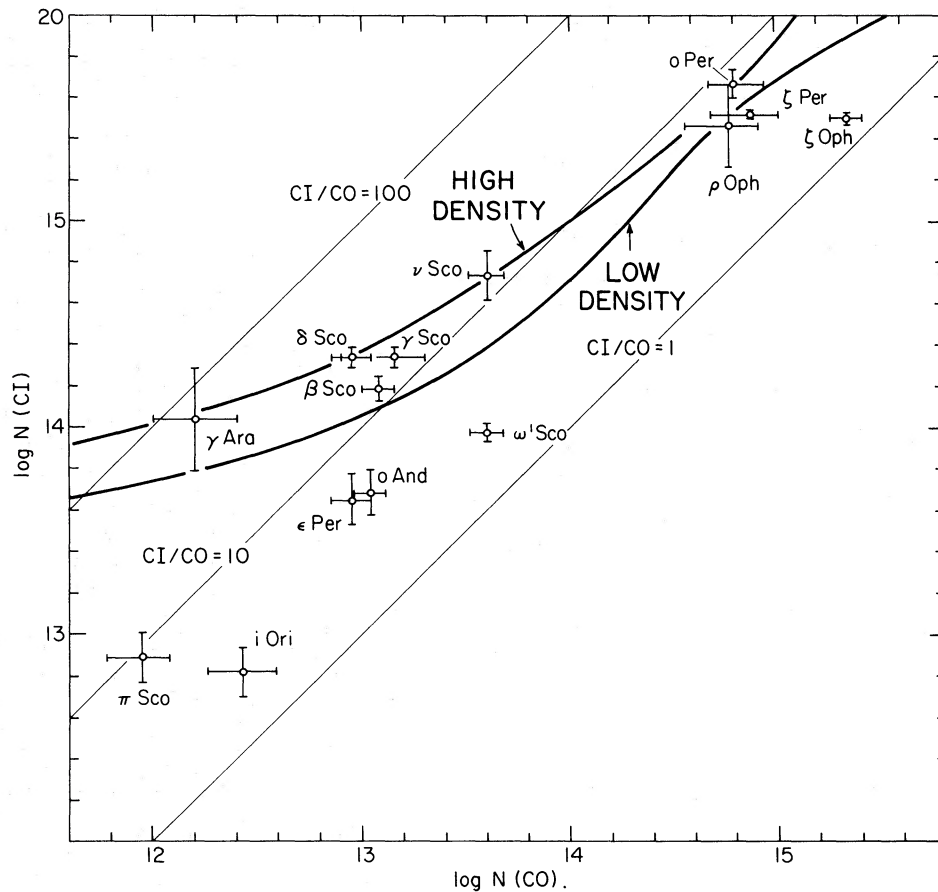


FIG. 4.—C I and CO column densities in a log-log plot. The data are from Table 1. *Light solid lines*, lines of constant C I/CO ratios. *Heavy solid curves*, the theoretical calculations used in Figs. 2 and 3 and discussed in the text. Note that the number on the top left should be 16, not 20.

densities increase rapidly with  $N(\text{H}_2)$  roughly as the second power. Finally, the detections appear to break into two groups, one with  $10^{12} \text{ cm}^{-2} < N(\text{CO}) < 4 \times 10^{13} \text{ cm}^{-2}$ , and the other (made up of  $\rho$  Oph,  $\zeta$  Per,  $\zeta$  Oph, and  $\rho$  Oph) with  $N(\text{CO}) \sim 10^{15} \text{ cm}^{-2}$ . Future observations may of course fill in the gap between these groups. In citing these trends, it must be noted that the data have a good deal of scatter and that they cover only  $1\frac{1}{2}$  decades in  $\text{H}_2$  column density. Clouds with the same  $N(\text{H}_2)$  can have different amounts of CO because they differ in some physical way, such as density, temperature, radiation field, evolutionary history, etc. Also, the empirical result that  $N(\text{CO})$  varies roughly as  $N(\text{H}_2)^2$  is strongly based on the four stars in the upper group. The lower column densities are consistent with a slope intermediate between 1 and 2.

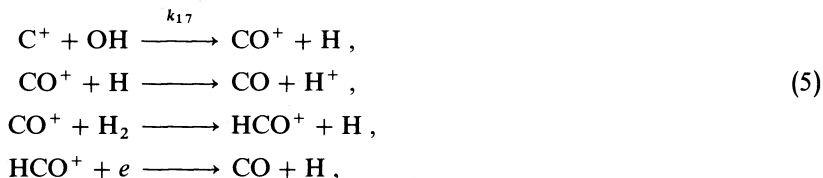
TABLE 2  
THEORETICAL MODEL PARAMETERS

Parameter	Low Density	High Density
Mean temperature (K) .....	55	30
Temperature range (K) .....	30–75	25–35
Mean density ( $\text{cm}^{-3}$ ) .....	150	2500
Density range ( $\text{cm}^{-3}$ ) .....	70–300	2000–3000
Cosmic ray ionization rate ( $\text{s}^{-1}$ ) .....	$10^{-17}$	$10^{-17}$
Carbon abundance .....	$2.5 \times 10^{-4}$	$2.5 \times 10^{-4}$
Oxygen abundance .....	$3.5 \times 10^{-4}$	$3.5 \times 10^{-4}$
$G_0(\text{C})^a$ ( $\text{s}^{-1}$ ) .....	$3.6 \times 10^{-10}$	$3.6 \times 10^{-10}$
$G_0(\text{CO})^a$ ( $\text{s}^{-1}$ ) .....	$2 \times 10^{-11}$	$2 \times 10^{-11}$
$G_0(\text{OH})^a$ ( $\text{s}^{-1}$ ) .....	$5.0 \times 10^{-10}$	$5.0 \times 10^{-10}$

<sup>a</sup> The parameters  $G_0$  are photodestruction rates appropriate to a typical location in the unshielded interstellar medium.



(The nomenclature for the rate constant is that of Glassgold and Langer 1976.) CO is then made from  $C^+$  by the reactions



or by neutral reactions with O at high densities. Another scheme which may be important at high densities is the *radiative association chemistry* of Black and Dalgarno (1973). Here the progenitor reaction is the radiative association of  $C^+$  with  $H_2$ ; CH is then produced by a sequence analogous to (4), and CO is made by the neutral reaction of O and CH. For purposes of simplicity we largely ignore radiative association from this qualitative discussion, although it is included in the numerical calculations.

The other essential features of the diffuse cloud chemistry are: (1)  $H^+$  is produced by cosmic rays, (2) OH and CO are destroyed mainly by radiation, although particle reactions can become important for thicker clouds or higher densities. When these processes are included, the following approximate expression for the CO density is obtained (Glassgold and Langer 1976):

$$\begin{aligned} n(\text{CO}) \approx & \frac{\zeta(f)B[T, f, x_e, x(\text{O})]}{G_0(\text{OH})(e^{-\tau(\text{OH})/n} + k_{17}x(\text{C}^+) + \dots)} \\ & \times \frac{\kappa x(\text{C}^+)}{G_0(\text{CO})(e^{-\tau(\text{CO})/n} + k_{25}x(\text{He}^+) + \dots)}. \end{aligned} \quad (6)$$

The notation used in this equation is:  $x(\text{O})$  and  $x(\text{C}^+)$  are the fractional abundances of O I and C II relative to  $n = n(\text{H}) + 2n(\text{H}_2)$ —close to the total gaseous abundances of oxygen and carbon;  $\zeta(f)$  is the rate of production of  $H^+$  by cosmic rays and  $f = 2n(\text{H}_2)/n$  (for  $f \rightarrow 0$ ,  $\zeta$  is the rate for  $p + H \rightarrow H^+ + e + p'$ );  $G_0(\text{OH})$  and  $G_0(\text{CO})$  are the photodissociation rates for OH and CO for the mean interstellar radiation field;  $\tau(\text{OH})$  and  $\tau(\text{CO})$  are the optical depths for attenuation of the dissociating radiation, largely due to absorption by dust grains;  $B$  is a series of branching ratios which enter at each step of the chain described by equations (3) and (4) starting with  $H^+$  and ending with OH (the consequences of the dependence of  $B$  on  $T, f, x(\text{O})$ , and the electron fraction  $x_e$  will be discussed below);  $\kappa$  is an effective rate constant for the production of CO according to equation (5); and  $k_{25}$  is the rate constant for the reaction whereby CO is destroyed by  $\text{He}^+$ ,  $\text{He}^+ + \text{CO} \rightarrow \text{C}^+ + \text{O} + \text{He}$ . In the destruction denominators of equation (6), only the leading processes have been indicated.

Two simple conclusions about the density of CO can be deduced from equation (6) in the limit of thin, dilute clouds:  $n(\text{CO})$  varies with density as  $n^2$ , and exponentially with thickness ( $\exp[\tau(\text{OH}) + \tau(\text{CO})]$ ). The density dependence is actually  $n(\text{H}_2)^2$  because, in the indicated limit, the factor  $B$  is proportional to  $f^2$ —there being two reactions involving  $H_2$  in equation (4). These simple dependences are easily obscured in the actual model calculations which involve inhomogeneous density, temperature, and abundance profiles, and which plot column densities rather than local densities. Even more important is the transition to a regime where molecule destruction is dominated by particle reactions, rather than radiation. Although this does not occur for CO for clouds with thickness

$$A_v \lesssim 0.58 \ln \left( \frac{G_0(\text{CO})}{k_{25}n(\text{He}^+)} \right) \sim 2,$$

a result which is independent of density because  $n(\text{He}^+)$  is,  $C^+$  does destroy OH more rapidly than radiation if

$$n > 2000 e^{-1.75A_v} \text{ cm}^{-3}.$$

Where this condition is satisfied, the CO density dependence is linear and the exponential growth is halved. Other effects also conspire to reduce the growth of CO with density and thickness, e.g.  $\zeta(f) \propto 1 - f$  and  $B \propto e^{-232/T}$ , and  $f$  increases and  $T$  decreases going into a cloud. In calculations which appear suitable for clouds with CO column densities in the range  $10^{12}$ – $10^{15} \text{ cm}^{-2}$ ,  $N(\text{CO})$  varies with  $N(\text{H}_2)$  more like the first than the second power.

Let us now examine the correlations noted in Figure 1 in the context of the theoretical calculations. In Figure 2 we plot the column densities from Figure 1 (except for  $\iota$  Ori) together with the low and high density model calculations. Except for 67 Oph, the two theoretical curves reasonably bracket most of the data. The four directions with large CO column densities appear to cluster near the high density curve, whereas the rest of the data tend to lie closer to the low density curve. A reasonable qualitative fit to the overall trend of the data could be achieved by a curve midway between the two in Figure 3. If abundances, radiation field, and cosmic ray ionization rate were held fixed at the values given in Table 2, the mean density would be about  $1000 \text{ cm}^{-3}$ .

The best-fit straight line fit to all of the data in Figure 2 is closer to a quadratic than a linear dependence. There may not be a great deal of significance to this result because there are two groups of data, and a single line does not give a

particularly good fit to both. The near quadratic dependence is being forced by the high-CO group; the low-CO group might be better described by an intermediate slope  $\sim \frac{3}{2}$ . The theoretical calculations also support an intermediate slope for clouds with  $N(\text{H}_2) > 2 \times 10^{19} \text{ cm}^{-2}$ .

### c) CO and Total Hydrogen

Figure 3 is a log-log plot of the column density of CO versus total hydrogen,  $N = N(\text{H}) + 2N(\text{H}_2)$ . Both the atomic and molecular hydrogen column densities have been determined by *Copernicus* measurements of UV absorption lines. The H I observations are based on the saturated  $\text{L}\alpha$  line, so it is impossible to correlate the velocities of the atomic and molecular hydrogen features. Much of the H I may be distributed fairly uniformly along the line of sight toward the star. It may have little to do with the gas inside a molecular clump, or with the attention of dissociating UV radiation. For this reason we have included both  $2N(\text{H}_2)$  and  $N(\text{H}) + 2N(\text{H}_2)$  in Figure 3, using a small dot for the former and a large circle for the latter and connecting the two by a light horizontal line. The small dot for  $2N(\text{H}_2)$  may be considered as the minimum column density of gas associated with the CO.

The CO column densities appear very differently when plotted versus  $N$  (Fig. 3) instead of  $N(\text{H}_2)$  (Fig. 1). CO upper limits for low- $N(\text{H}_2)$  clouds now appear in the same portion of Figure 3 as detections, a situation highlighted by the light horizontal lines. The bare detection for  $\iota$  Ori now appears much less anomalous than in Figure 1. It seems clear that  $\text{H}_2$  is a better discriminant between various groups of CO column densities than is total hydrogen.

The solid curves are the theoretical calculations discussed in § IIIb. They rise quite rapidly at first due to the dependence of  $n(\text{CO})$  on  $n(\text{H}_2)$ . The effect is accentuated in the present representation because the molecular hydrogen fraction  $f$  is itself a strongly increasing function of  $N$  due to self-shielding in the Lyman band lines (Hollenbach, Werner, and Salpeter 1971), at least below a characteristic transition thickness  $N_{\text{tr}}(\text{H}_2)$  (Federman, Glassgold, and Kwan 1979). As  $N$  increases, the growth rate of CO decreases somewhat because of the gradual saturation of  $\text{H}_2$  and because of various changes in the chemistry discussed above. For larger values of  $N \sim 10^{21} \text{ cm}^{-2}$ ,  $N(\text{CO})$  increases exponentially because of dust attenuation. Eventually the rapid growth of CO saturates because of substantial conversion of  $\text{C}^+$  into C and CO, which occurs for clouds with several magnitudes of visual extinction (Glassgold and Langer 1975).

At first sight the two theoretical calculations do not appear to bracket the observations in Figure 3 as well as they did in Figures 1 and 2. There is considerable uncertainty in locating the data points in Figure 3 because of our ignorance about the location of the H I. Except for a few cases, this uncertainty is about the size of the horizontal separation of the two curves, which have been computed for rather different densities (of Table 2). Most of the observations falling to the right of the low density curve in Figure 3 correspond to directions where large amounts of H I have been observed. If a considerable fraction of the H I were *not* associated with the CO, then the data might be within, or at least close to, the region bounded by the two theoretical curves. It is particularly noteworthy that most of the measurements to the right of the low density curve are in the Oph-Sco region of the sky, where large sheets of H I are believed to exist. For example, Crutcher (1976) analyzed observations for two stars in this region,  $\zeta$  Oph and  $\sigma$  Sco, using 21 cm observations as well as UV and optical absorption line measurements, very much in the spirit of Herbig's classic work on  $\zeta$  Oph (Herbig 1968). Assigning only a small fraction of the H I along the line of sight to the densest interstellar cloud, Crutcher obtained the following column densities for the clouds:  $N(\zeta \text{ Oph cloud}) \approx 1.0 \times 10^{21} \text{ cm}^{-2}$  (in contrast to  $1.4 \times 10^{21} \text{ cm}^{-2}$  from Table 1) and  $N(\sigma \text{ Sco cloud}) \approx 8.2 \times 10^{20} \text{ cm}^{-2}$  (in contrast to  $2.3 \times 10^{21} \text{ cm}^{-2}$  from Table 1). Using these values in Figure 3 would shift the data points for  $\zeta$  Oph and  $\sigma$  Sco close to the high and low density curves, respectively. Similar shifts are probably appropriate for most of the other stars to the right of the low density curve in Figure 3, especially  $\rho$  Oph. Therefore, when account is taken of the uncertainty in the value of  $N$ , there is rough agreement between the theory and observations with regard to the general increase of  $N(\text{CO})$  with  $N$ . A more detailed comparison would be inappropriate until the basic problem of the location of the H I along the line of sight can be settled by observational means.

The crosses in Figure 3 are the closely related radio observations of Knapp and Jura (1976), who reported detections at 2.6 mm toward 11 bright stars with  $N(^{12}\text{CO}) \geq 6 \times 10^{14} \text{ cm}^{-2}$ . For three directions where CO also is detected in the UV ( $\sigma$  Per,  $\rho$  Oph, and  $\zeta$  Oph), the CO column densities, estimated on the assumption that the 2.6 mm emission is unsaturated, are typically about 50% larger than those given in Table 1. Considering that some CO may lie behind the stars, the two sets of results agree to within the uncertainties in the measurements. Atomic and molecular hydrogen measurements have been made for only one other star ( $\lambda$  Cep) in their list, all of which involve heavily reddened ( $0.33 < E_{BV} < 0.64$ ) lines of sight. The gas to dust ratio for  $\lambda$  Cep is  $4.4 \times 10^{21} \text{ cm}^{-2} \text{ mag}^{-1}$ , about 25% less than the mean for the large *Copernicus* survey of Bohlin, Savage, and Drake (1978). We have plotted the eight additional data of Knapp and Jura in Figure 3 by converting the known values of the selective extinction with the above mentioned mean value,  $\langle N \rangle / \langle E_{BV} \rangle = 5.8 \times 10^{21} \text{ cm}^{-2} \text{ mag}^{-1}$ . These values are represented by crosses without error bars; the errors must be at least  $\pm 0.3$  dex.

Considering that some of the emission may arise beyond the stars, the radio of Knapp and Jura appear somewhat low, except for the indicated lower limit for HD 21483. Perhaps the column densities have been underestimated because of unsuspected saturation or multiple-clumping effects. It also must be borne in mind that there is no way of knowing the exact amount of gas and/or dust coexistent with the CO. Thus the crosses in Figure 3 might be shifted toward the left, as is illustrated for the case of  $\lambda$  Cep using UV data. The small dot is  $2N(\text{H}_2)$ , which might be the minimum hydrogen column density associated with the line of sight; and the cross is  $N(\text{H}) + 2N(\text{H}_2)$ . For the remaining observations, the best that

can be done for these lines is to use the value  $\langle 2N(\text{H}_2) \rangle / \langle E_{\text{BV}} \rangle = 1.34 \times 10^{21} \text{ cm}^{-2} \text{ mag}^{-1}$  determined for the 33 directions in the survey of Bohlin *et al.* which have  $E_{\text{BV}} > 0.3$ . If the crosses are placed in Figure 3 according to this rule, they are shifted just to the left of the high density theoretical curve. We conclude that the 2.6 mm observations of  $^{12}\text{CO}$  toward bright stars by Knapp and Jura are in reasonable agreement with the theory. In § IV we will discuss related radio observations of CO in dark clouds.

#### d) C I and CO

Figure 4 is a log-log plot of C I and CO column densities. For comparison we show (light) lines for which the ratio C I/CO is constant, as well as the high and low density theoretical calculations. The line for which  $N(\text{C I})/N(\text{CO}) = 10$  provides a rough order of magnitude fit for most diffuse clouds.

Theory predicts that the C I/CO deviates from a straight line with unit slope. For thin clouds [ $N(\text{CO}) < 10^{13} \text{ cm}^{-2}$ ], CO is a more rapidly varying function of cloud thickness than is C I because of the dependence of CO on  $\text{H}_2$ , discussed above. This results in the swing of the theoretical curves toward larger C I/CO ratios at the left of Figure 4. For thicker clouds [ $N(\text{CO}) > 10^{14} \text{ cm}^{-2}$ , to the right in Fig. 4], the opposite effect occurs because of the double dependence of the CO column density on dust optical depth in equation (6), as compared to C I which varies as  $\exp[\tau(\text{C I})]$ . In this regime, the high and low density curves differ in this respect because of the relatively greater importance of particle reactions in destroying OH at high densities.

The actual values of the C I/CO density ratio can be calculated approximately by combining the gas phase chemistry for CO described in § IIIb with radiative recombination-photoionization theory for C I. Ignoring the particle reaction contributions to the destruction denominators in equation (6), the following simple result is obtained for thin, dilute clouds:

$$\frac{n(\text{CO})}{n(\text{C I})} \approx \left( \frac{\alpha x_e}{\kappa} \right) \frac{G_0(\text{OH})G_0(\text{CO})}{B\zeta G_0(\text{C})} \exp[\tau(\text{C}) - \tau(\text{CO}) - \tau(\text{OH})]. \quad (7)$$

This result suggests that the C/CO ratio is not very sensitive to density, and this is borne out by the numerical calculations. Despite the fact that the densities in the two calculations differ by a factor which varies from 10 to 30, the C/CO ratios differ by less than a factor of 2. For thinner clouds, the  $f$  dependence of  $B$  causes C/CO to increase, whereas for thicker clouds C/CO decreases because of the exponential dust factor in equation (7).

The overall position of the theoretical curves in Figure 4 is controlled by many factors, as is evident from equation (7): cosmic ray ionization rate, radiation field intensity near 1000 Å, photodestruction rates, dust absorption and scattering properties, oxygen and carbon abundances, etc. Reasonably good values (accurate to within factors of 2–5) of these parameters have been determined by a number of investigations over the last several years. About the only difference between the parameters in Table 2 and those used before (e.g., in Gerola and Glassgold 1978) is that the depletion of carbon has been reduced from about 5 to 2. The photoionization rate for C has been increased to  $G_0(\text{CO}) = 3.6 \times 10^{-10} \text{ s}^{-1}$  on the basis of the theoretical calculation of Burke and Taylor (1979); Jura's calculation of the interstellar radiation field (Jura 1974) has been used for all photodestruction rates. The general trend of the data in Figure 4 appears to be reasonably well accounted for by current ideas on the synthesis of CO in the gas phase and standard recombination-photoionization theory for C.

It is somewhat disappointing that the data for the thinner clouds are so scattered. About a half-dozen clouds appear to conform with the upward swing of the theory to the left in Figure 4, but almost the same number appear to favour a constant ratio of about 10. The gas phase theory makes a very definite prediction here, based on the occurrence of the hydrogen abstraction reactions  $\text{O}^+ + \text{H}_2 \rightarrow \text{OH}^+ + \text{H}$  and  $\text{OH}^+ + \text{H}_2 \rightarrow \text{OH}_2^+ + \text{H}$ . By contrast, grain chemistry would predict a constant C I/CO ratio for thin clouds (although it would have difficulties in explaining the actual values). It would be of great interest to have more extensive observations of interstellar clouds with relatively small amounts of CO ( $10^{11}$ – $10^{13} \text{ cm}^{-2}$ ) and C I ( $10^{12}$ – $10^{14} \text{ cm}^{-2}$ ).

#### IV. COMPARISON OF CO IN DIFFUSE AND DARK CLOUDS

In the previous section we discussed the results of our UV survey of CO in diffuse clouds toward nearby bright stars. The thickness of these clouds ranges up to about 1 visual magnitude. Many observations have been made of CO by observing emission from its rotational lines, generally with clouds thicker than  $A_v = 1$ . These clouds fall into two broad types, large cloud complexes associated with regions of massive star formation, and dark clouds (Barnard objects) which usually show no sign of massive star formation. It is very difficult to measure the abundance of CO in the large cloud complexes, mainly because the lines are heavily saturated and also because there is no way to measure the main hydrogen component of the gas. These problems are alleviated in many dark clouds where it is at least possible to measure the dust by counting stars. Many of these clouds have thicknesses of the same order or only several times larger than the thickest diffuse clouds. It is therefore of interest to compare the abundance of CO in diffuse and dark clouds.

Dickman (1978) measured the ratio of  $^{13}\text{CO}$  to dust at more than 100 locations in 38 dark clouds by combining radio observations of  $^{12}\text{CO}$  and  $^{13}\text{CO}$  with sar counts of red and blue plates. Only the data for  $1.0 \lesssim A_v \lesssim 4$  are reliable, from

which Dickman deduced the result

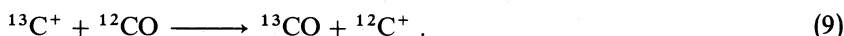
$$\left\langle \frac{A_v}{N(^{13}\text{CO})} \right\rangle = (4 \pm 2) \times 10^{-16} \text{ mag cm}^2. \quad (8a)$$

Using the latest "standard" values for the gas to dust ratio  $\langle N \rangle / E_{BV} = 5.8 \times 10^{21} \text{ cm}^{-2} \text{ mag}^{-1}$  (Bohlin, Savage, and Drake 1978), and for  $R = \langle A_v \rangle / \langle E_{BV} \rangle = 3.1$  (Savage and Mathis 1979), (8a) becomes

$$\frac{\langle N(^{13}\text{CO}) \rangle}{\langle N \rangle} \approx (1.3 \pm 0.7) \times 10^{-6}, \quad (8b)$$

very close to Dickman's published value. This last result is based on the assumption that dust properties (specifically the gas to dust ratios) are the same in dark clouds as in diffuse clouds. Similar studies have been made for many locations in the dark cloud L63 (Elmegreen and Elmegreen 1979; Snell 1979; Strohacker 1978), which confirm Dickman's result, i.e.,  $^{13}\text{CO}$  and  $A_v$  are linearly related for  $1 \lesssim A_v \lesssim 4$ . The latter authors give a value for the ratio (8a) which is about 70% larger than Dickman's, equivalent to an abundance ratio in (8b) of  $(7.5 \pm 2.5) \times 10^{-7}$ .

The ratio  $N(^{12}\text{CO})/N(^{13}\text{CO})$  must be known before CO observations in diffuse and dark clouds can be compared. It is well known that this ratio in giant molecular clouds is less than the terrestrial value of 89; the best current estimate for such clouds is  $60 \pm 20$  (Penzias 1979). One possible reason for the reduction is chemical fractionation, e.g., through the gas-phase exchange reaction (Watson, Huntress, and Anicich 1979)



Because this reaction is only slightly exothermic (by about 35 K), fractionation is important only for cold regions of clouds. Langer (1977) also showed that the fractionation effect is largest for cloud thicknesses (or depths into a very large cloud) characterized by  $A_v \sim 2-3$ . Langer *et al.* (1980) have recently demonstrated this effect with high sensitivity and high resolution studies of the radio emission from  $^{13}\text{C}^{16}\text{O}$  and  $^{12}\text{C}^{18}\text{O}$  in the dark clouds B5, B335, and L1262. Thus chemical fractionation plays a large role in the conversion of  $^{13}\text{CO}$  to  $^{12}\text{CO}$  abundances in dark clouds.

We have calculated the fractionation effect of equation (9) for the high and low density theoretical curves (§ IIIc), and Table 3 presents a short table of these results. There is a big difference between high and low densities because fractionation must compete with other reactions of  $\text{C}^+$  in order to be important. In very diffuse clouds the chemical reactivity is determined by the UV radiation field, whose effects are proportional to  $G(X)/n$ . Thus fractionation will be less important at low densities.

Figure 5 compares Dickman's measurements and the results of this paper by plotting the ratio  $N(^{13}\text{CO})/N(\text{H}_2)$  versus  $N(\text{H}_2)$ . The large set of Dickman's data is represented by a box with dashed lines which contains those points which lie within a range  $\pm 50\%$  about the mean value. It is assumed with Dickman that full conversion to molecular hydrogen has occurred in the dark clouds. The narrow rectangle is a similar representation of observations of the dark cloud L63 which lie in the range  $A_v = 1-5$  (Snell 1979; Strohacker 1978). The solid line marked diffuse clouds is an empirical fit to our results:

$$N(\text{CO}) = 6.30 \times 10^{13} \text{ cm}^{-2} [N(\text{H}_2)/10^{20} \text{ cm}^{-2}]^2, \quad (10)$$

which has been corrected for fractionation by interpolation on Table 3. The short extension (*dots*) of the diffuse cloud line goes to within  $\frac{1}{2}$  dex of the centroids of the dark cloud results. Column densities of CO for diffuse and dark clouds appear to form a continuum for  $N(\text{H}_2)$  in the range  $10^{19}-10^{22} \text{ cm}^{-2}$ .

In an earlier discussion of Figure 3 [ $N/(\text{CO})$  versus  $N$ ] we noted how uncertain the value of  $N$  is because of our ignorance about the location of the H I along the line of sight. Similar difficulties exist in representing the dark cloud

TABLE 3  
FRACTIONATION OF  $^{13}\text{CO}$ <sup>a</sup>

$A_v$	$N(^{12}\text{CO})/N(^{13}\text{CO})$	
	Low Density	High Density
0.5 .....	80	34
1.0 .....	75	28
1.5 .....	60	20
2.0 .....	46	10
2.5 .....	34	
3.0 .....	24	

<sup>a</sup> Terrestrial value for  $^{12}\text{C}/^{13}\text{C} = 89$ .  
 $A_v = N(2 \times 10^{21} \text{ cm}^{-2})^{-1} \text{ mag}$ .

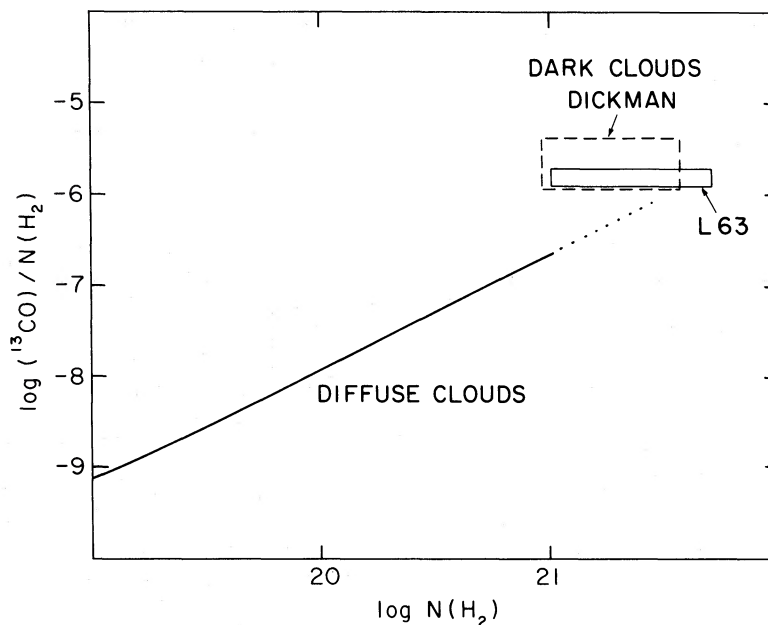


FIG. 5.—Comparison of  $^{13}\text{CO}$  in diffuse clouds (solid line) and dark clouds (boxes). The solid line is a fit to the results of this paper corrected for fractionation.

results in Figure 5. The extinction determined by star counts may include regions along the line of sight without CO, so that some of the dark cloud data may have been placed too far to the right in Figure 5. Beam dilution may lead to the opposite error for dark cloud measurements for  $A_v \approx 1$ .

In demonstrating the concordance between diffuse and dark cloud measurements of CO, the fractionation reaction (9) plays an important role. According to Table 3 and the earlier results of Langer (1977), fractionation is large in the thicker diffuse clouds like  $\zeta$  Oph and is at its peak for the cool, dark clouds observed by Dickman.

Little is known about the abundance of CO for  $N(\text{H}_2) > 10^{22} \text{ cm}^{-2}$  for the reasons given at the beginning of the section. Abundance studies of the dense cores of molecular clouds (Wootten *et al.* 1978) indicate that CO and other molecular abundances (relative to total hydrogen) decrease with increasing density at very high densities. The  $N(^{13}\text{CO})/A_v$  ratio for L43 also decreases with increasing  $A_v > 4$  according to Elmegreen and Elmegreen (1979), who made star counts with infrared plates. These results suggest that the CO abundance may actually peak for cool, dark clouds of intermediate density, i.e., for clouds of the type studied by Dickman.

A full understanding of the CO abundance is important for a quantitative analysis of the physical and dynamical properties of molecular interstellar clouds. One important application is to estimates of mass. For example, Solomon and Sanders (1980) estimate that the mean mass of a giant molecular cloud is  $5 \times 10^5 M_\odot$ , that the total mass involved in the galactic ensemble of such clouds is  $2 \times 10^9 M_\odot$ , and that about 90% of the gas in the "molecular ring" between 4 and 8 kpc is in molecular form. In obtaining these results, they take the ratio  $N(^{13}\text{CO})/N$  to be  $2.5 \times 10^{-7}$ , about five times smaller than (the revised) Dickman's result in equation (8b). Blitz and Shu (1980) have emphasized that the mass estimates of Solomon and Sanders may be too large because they use too small a CO abundance. The crucial question in estimating masses of giant molecular clouds is whether it is valid to apply Dickman's (or any other) results for nearby dark clouds to molecular clouds in general. A closely related question is whether the dust to gas ratio inside large clouds is the same as those determined along lines of sight to nearby bright stars. Another complication is the effect of C and O abundance gradients, which might be expected to decrease in moving away from the center of the Galaxy (Mezger 1979). Giant molecular clouds may well be complexes of clouds with properties similar to dark clouds (Blitz and Shu 1980), but the basic assumptions used in mass estimates need to be confirmed by observations. The results of this paper suggest that the  $^{13}\text{CO}$  abundance is a fairly strong function of density, thickness, and temperature. Use of a fixed abundance in giant cloud complexes must be an oversimplification.

#### V. CONCLUSION

We have presented an overall picture of CO column densities on the basis of *Copernicus* observations of UV absorption lines. Comparison of the results with similar measurements of  $\text{H}_2$  and C I prove to be very useful, more so than the total hydrogen along the line of sight  $N = N(\text{H}) + 2N(\text{H}_2)$ . The observed CO column densities are in the range  $10^{12}$ – $10^{15} \text{ cm}^{-2}$  for clouds with  $\text{H}_2$  column densities in the range  $10^{19}$ – $10^{21} \text{ cm}^{-2}$ . The CO and  $\text{H}_2$  column densities are empirically related by a rough quadratic law, given in equation (10). The UV measurements have also been compared with radio

observations of CO for both cool, dark clouds and for heavily reddened lines of sight toward early type stars. The radio and UV observations form a single continuum when plotted against the H<sub>2</sub> content of the clouds.

Comparisons also have been made with isobaric cloud models containing a full description of gas phase, ion-molecule interstellar chemistry. The overall trends of the CO data can be reproduced, or at least bracketed, by typical low and high density calculations. In particular the data show two important phenomena predicted by the theory. For thin clouds, the CO abundance is controlled by the abundance of H<sub>2</sub>, and for thicker clouds by the attenuation of dissociating UV radiation by dust.

Significant limitations exist in determining CO abundances, whether radio or UV methods are used. For radio observations [applicable for  $N(\text{CO}) \geq 10^{15} \text{ cm}^{-2}$ ], there is no direct way of measuring the total hydrogen density of the emitting regions. The best that has been done so far is to measure the dust thickness by counting stars, a technique feasible for  $1 < A_v < 5$ , and to convert to total hydrogen thickness by adopting a "standard" dust to gas ratio (determined toward bright stars). We have emphasized that a similar but probably less severe difficulty exists for the UV data. Here the problem is to establish what fraction of the H I coexists with the molecular clumps. Without additional observational information, our solution to the problem involves correlating CO with H<sub>2</sub> or other coexisting, recombined species such as C I.

Both the radio and UV lines are readily saturated, and the only sure way of dealing with this problem is to measure weak lines. In the radio region this means working with <sup>13</sup>C<sup>16</sup>O or preferably <sup>12</sup>C<sup>18</sup>O. In the UV, measurements of the A-X band, which lies shortward of 1544 Å, would be ideal because the oscillator strength decreases rapidly with  $\nu'$  from the maximum value at  $\nu' = 2$ . Such measurements, if carried out with spectral resolution sufficient to resolve the rotational structure (i.e.,  $< 0.05 \text{ \AA}$ ), also would provide the curve of growth essential for determining column densities.

Improved UV observations of CO at higher sensitivity and spectral resolution would answer some of the questions raised by our data. Localization in velocity space of the various interstellar features would permit an identification of those species which correlate with CO. Measurements with increased sensitivity would determine whether CO exists in clumps with small amounts of molecular hydrogen, a question raised by our putative detection of CO for  $\iota$  Ori and by the variation in the C I/CO ratio for thin clouds. Similarly, higher sensitivity observations would permit detection of CO toward more heavily reddened stars than those accessible in this *Copernicus* survey ( $E_{BV} < 0.33$ , except for  $\rho$  Oph which has  $E_{BV} = 0.47$ ). The CO column density regime between  $\sim 10^{15}$  and  $10^{17} \text{ cm}^{-2}$  has particular physical interest: it is here that increased shielding of UV radiation induces a transition in carbon from C II, its diffuse interstellar phase, into C and CO, the dense interstellar phases—with accompanying changes in the ionization and thermal properties of the medium (Glassgold and Langer 1975, 1976). This region is also the interface between radio and UV investigations of CO in interstellar clouds.

The success of the theory in explaining overall trends in the data suggests that more detailed analysis might explain deviations of particular clouds from the average. Only a few case studies of individual directions have been carried out so far ( $\zeta$  Oph [Black and Dalgarno 1977];  $\zeta$  Per [Hartquist, Black, and Dalgarno 1978; Hartquist 1978]; and  $\gamma$  Ara [Federman and Glassgold 1980]), and none has involved a complete line of sight analysis. In such studies, the tacit assumption is usually made that all of the gas and dust is associated with the molecular clumps. Because the exact locations of the H I and the dust are largely unknown, this assumption is clearly unfounded. In the present work we adopted a different approach, which was to analyze the CO observations in terms of closely related species, such as H<sub>2</sub> and C I, which may be expected to coexist with the heavier molecules. The empirical and theoretical correlations of the data appear to support this point of view.

Many of the issues raised in this article will eventually be clarified by further observations with new techniques. Already important data on neutral carbon are becoming available through the discovery of the 610  $\mu\text{m}$  fine structure line in emission from large molecular clouds (Phillips *et al.* 1980). These observations bear directly on the transition region between ionized carbon and neutral carbon and CO, and on the nature of the interstellar carbon chemistry in dense clouds. The infrared absorption spectrum of CO may also prove to be an important diagnostic tool, as emphasized by Black (1980) and demonstrated by the observation of the 1-0 absorption band of CO toward the Becklin-Neugebauer object in Orion (Hall *et al.* 1978).

This work has been supported by NASA grant NGR-33-016-196 at New York University and by contract NAS 5-23576 at Princeton University.

#### REFERENCES

- Black, J. H. 1980, private communication.  
 Black, J. H., and Dalgarno, A. 1973, *Ap. Letters*, **15**, 79.  
 ———. 1977, *Ap. J. Suppl.*, **34**, 405.  
 Blitz, L., and Shu, F. 1980, *Ap. J.*, **238**, 148.  
 Bohlin, R. C. 1975, *Ap. J.*, **200**, 402.  
 Bohlin, R. C., Savage, B. D., and Drake, J. F. 1978, *Ap. J.*, **224**, 132.  
 Burke, P. G., and Taylor, K. T. 1979, *J. Phys.*, **B12**, 297.  
 Cowie, L., Songaila, A., and York, D. G. 1979, *Ap. J.*, **230**, 469.  
 Crutcher, R. M. 1976, *Ap. J.*, **208**, 382.  
 Dalgarno, A., and Black, J. H. 1976, *Rept. Progr. Phys.*, **39**, 573.  
 Dickman, R. L. 1978, *Ap. J. Suppl.*, **37**, 407.  
 Elmegreen, D. M., and Elmegreen, B. G. 1979, *A.J.*, **84**, 615.  
 Elmegreen, B. G., Lada, C. J., and Dickinson, D. F. 1979, *Ap. J.*, **230**, 415.  
 Federman, S. R., and Glassgold, A. E. 1980, *Astr. Ap.*, in press.  
 Federman, S. R., Glassgold, A. E., and Kwan, J. 1979, *Ap. J.*, **227**, 446.  
 Gerola, H., and Glassgold, A. E. 1978, *Ap. J. Suppl.*, **37**, 1.  
 Glassgold, A. E., and Langer, W. D. 1974, *Ap. J.*, **193**, 73.  
 ———. 1975, *Ap. J.*, **197**, 347.

- . 1976, *Ap. J.*, **206**, 85.
- Gordon, M. A., and Burton, W. B. 1976, *Ap. J.*, **208**, 346.
- Hall, D. L. L., Kleinmann, S. G., Ridgway, S. T., and Gillett, E. C. 1978, *Ap. J. (Letters)*, **223**, L47.
- Hartquist, T., Black, J. H., and Dalgarno, A. 1978, *M.N.R.A.S.*, **185**, 643.
- Herbig, G. 1968, *Zs. Ap.*, **68**, 243.
- Hesser, J. E. 1968, *J. Chem. Phys.*, **48**, 2518.
- Hollenbach, D., Werner, M. W., and Salpeter, E. E. 1971, *Ap. J.*, **163**, 155.
- Jenkins, E. B., Drake, J. F., Morton, D. C., Rogerson, J. B., Spitzer, L., and York, D. G. 1973, *Ap. J. (Letters)*, **181**, L122.
- Jenkins, E. B., and Shaya, E. J. 1979, *Ap. J.*, **231**, 55.
- Jura, M. 1974, *Ap. J.*, **191**, 375.
- Knapp, G. R., and Jura, M. 1976, *Ap. J.*, **209**, 782.
- Kutner, M. L., Tucker, K. D., Chin, G., and Thaddeus, P. 1977, *Ap. J.*, **215**, 521.
- Langer, W. D. 1977, *Ap. J. (Letters)*, **212**, L39.
- Langer, W. D., Goldsmith, P. F., Carlson, E. R., and Wilson, R. W. 1980, *Ap. J. (Letters)*, **235**, L39.
- Lassettre, E. N., and Skeberle, A. 1971, *J. Chem. Phys.*, **54**, 1957.
- Loren, R. B. 1979, *Ap. J. (Letters)*, **234**, L207.
- Mezger, P. 1979, private communication.
- Morton, D. C. 1975, *Ap. J.*, **197**, 85.
- . 1979, *M.N.R.A.S.*, **184**, 713.
- Morton, D. C., and Hu, E. 1975, *Ap. J.*, **202**, 638.
- Penzias, A. A. 1979, in *IAU Symposium 87: Interstellar Molecules*, ed. B. Andrew (Dordrecht: Reidel), in press.
- Phillips, T. G., Huggins, P. J., Kuiper, T. B. H., and Miller, R. E. 1980, *Ap. J. (Letters)*, **238**, L103.
- Pilling, M. J., Boss, A. M., and Brown, W. 1971, *J. Quant. Spectrosc. Rad. Transf.*, **11**, 1593.
- Savage, B. D., Bohlin, R. C., Drake, J. F., and Budich, W. 1977, *Ap. J.*, **216**, 291.
- Savage, B. D., and Mathis, J. S. 1979, *Ann. Rev. Astr. Ap.*, **17**, 73.
- Scoville, N. Z., and Solomon, P. M. 1975, *Ap. J. (Letters)*, **199**, L105.
- Scoville, N. Z., Solomon, P. M., and Penzias, A. A. 1975, *Ap. J.*, **201**, 352.
- Smith, A. M., and Stecher, T. P. 1971, *Ap. J. (Letters)*, **164**, L43.
- Smith, W. H. 1978, *Phys. Sci.*, **17**, 513.
- Snell, R. N. 1979, Ph.D. thesis, University of Texas at Austin.
- Snow, T. 1975, *Ap. J. (Letters)*, **202**, L87.
- . 1977, *Ap. J.*, **216**, 724.
- Snow, T., and Jenkins, E. B. 1980, preprint.
- Solomon, P., and Sanders, D. B. 1980, in *Giant Molecular Clouds in the Galaxy*, ed. P. Solomon and M. Edmunds (New York: Pergamon).
- Solomon, P. M., Scoville, N. Z., and Sanders, D. B. 1979, *Ap. J. (Letters)*, **232**, L89.
- Strohacker, O. C. 1978, M.A. thesis, University of Texas at Austin.
- Watson, W. D. 1976, *Rev. Mod. Phys.*, **48**, 413.
- Watson, W. D., Anicich, V. G., and Huntress, W. T., 1976, *Ap. J. (Letters)*, **205**, L165.
- Wilson, R. W., Jefferts, K. B., and Penzias, A. A. 1970, *Ap. J. (Letters)*, **161**, L43.
- Wooten, A., Evans, N. J., Snell, R., and Vanden Bout, P. 1978, *Ap. J. (Letters)*, **225**, L143.
- York, D. G. 1972, memo to users of *Copernicus data*, 1972, Dec. 8.
- York, D. G., and Miller, A. E. 1974, memo to users of *Copernicus data*, 1974 Dec. 9.

S. R. FEDERMAN: Department of Astronomy, University of Texas, Austin, TX 78712

A. E. GLASSGOLD: Physics Department, New York University, New York, NY 10003

E. B. JENKINS, Jr.: Princeton University Observatory, Princeton University, Princeton, NJ 08540

E. J. SHAYA: Department of Astronomy, 2505 Correa Road, University of Hawaii, Honolulu, HI 96822